

1 **Downregulated microRNA-130b-5p Prevents Lipid Accumulation and Insulin
2 Resistance in a Murine model of Nonalcoholic Fatty Liver Disease**

3 **Running title:** Roles of miR-130b-5p in NAFLD *via* IGFBP2

4

5 **Xiaonan Liu, Shuhong Chen, Lanju Zhang^{*}**

6 Department of Endocrinology, Linyi People's Hospital, Linyi 276003, P.R. China

7

8 *** Correspondence to:** Dr. Lanju Zhang, Department of Endocrinology, Linyi People's Hospital,
9 No. 27, Eastern Section of Jiefang Road, Lanshan District, Linyi 276003, Shandong Province, P.R.
10 China

11 **E-mail:** Zhanglanju111@163.com

12 **Tel.:** +86-0539-8216031

13

14 **ABSTRACT**

15 Nonalcoholic fatty liver disease (NAFLD) amplifies the risk of various liver diseases, ranging from
16 simple steatosis to non-alcoholic steatohepatitis, fibrosis and cirrhosis, and ultimately hepatocellular
17 carcinoma. Accumulating evidence suggests the involvement of aberrant microRNAs (miRNAs or
18 miRs) in the activation of cellular stress, inflammation and fibrogenesis in hepatic cells at different
19 stages of NAFLD and liver fibrosis. Here, we explored the potential role of miR-130b-5p in the
20 pathogenesis of NAFLD, including lipid accumulation and insulin resistance as well as the
21 underlying mechanism. Initially, the expression of miR-130b-5p and insulin like growth factor
22 binding protein 2 (IGFBP2) was examined in the established high-fat diet-induced NAFLD mouse
23 models. Then, the interaction between miR-130b-5p and IGFBP2 was validated using
24 dual-luciferase reporter assay. The effects of miR-130b-5p and IGFBP2 on lipid accumulation and
25 insulin resistance as well as the AKT pathway-related proteins were evaluated using gain- or
26 loss-of-function approaches. miR-130b-5p was upregulated and IGFBP2 was downregulated in
27 liver tissues of NAFLD mice. miR-130b-5p targeted IGFBP2 and downregulated its expression.
28 MiR-130b-5p inhibition or IGFBP2 overexpression reduced the expression of SREBP-1, LXRa,
29 ChREBP, SCD1, ACC1 and FAS, and levels of FBG, FINS and HOMA-IR while increasing the
30 ratio of p-AKT/AKT in NAFLD mice. Overall, downregulation of miR-130b-5p can prevent
31 hepatic lipid accumulation and insulin resistance in NAFLD by activating IGFBP2-dependent AKT
32 pathway, highlighting the potential use of anti-miR-130b-5p as therapeutic approaches for the
33 prevention and treatment of NAFLD.

34 **KEYWORDS:** Nonalcoholic fatty liver disease; MicroRNA-130b-5p; Insulin-like growth factor
35 binding protein 2; AKT pathway; Lipid accumulation; Insulin resistance

36

37 **INTRODUCTION**

38 Nonalcoholic fatty liver disease (NAFLD) is currently the principle cause of chronic liver
39 diseases in developed countries across the world (31). NAFLD has two initial manifestations, which
40 are nonalcoholic fatty liver disease (NAFL) and nonalcoholic steatohepatitis (NASH), which often
41 progresses to cirrhosis, liver failure, and even hepatocellular carcinoma (HCC) (8, 32, 33). NAFLD
42 is associated with hepatic lipid accumulation without excessive alcohol intake (22), which obstructs
43 the key physiological liver functions such as sugar and lipid metabolism (2). Moreover, insulin
44 resistance is a characteristic feature of NAFLD (5). microRNAs (miRNAs or miRs) have recently
45 emerged as novel biomarkers and therapeutic tools in the management of NAFLD due to their
46 major roles in gene regulation, with diverse influences in the maintenance of metabolic homeostasis,
47 particularly the states of obesity and insulin resistance (15, 40).

48 miRNAs are a class of endogenous small non-coding RNAs naturally encoded in the genome
49 of many species (7). Accumulating evidence has highlighted the diagnostic and prognostic
50 potentials of miRNAs in NAFLD (13) such as miR-34a and miR-122 (6). The upregulation of
51 miR-130b associated with liver tumor has been reported (28). More importantly, miR-130b
52 expression is elevated in mice following a high-fat diet (HFD) (35). The Targetscan, DIANA
53 TOOLS and miRDB websites predicted binding sites between miR-130b-5p and insulin-like growth
54 factor binding protein 2 (IGFBP2). The IGFBPs are a family of six proteins that function not only in
55 IGF transport, but are also involved in the tumorigenesis, development and resistance to therapies
56 (4). IGFBP2, a member of IGFBPs as well as a leptin-regulated gene, can improve glucose
57 metabolism and diminish insulin resistance in diabetes (18, 21). In addition, a previous study
58 suggested that IGFBP2 is differentially expressed in NAFLD (3), thus establishing it as a
59 therapeutic target in that disease. Furthermore, IGFBP2 has been reported to activate the protein
60 kinase B (AKT) pathway in glioma cells (14). AKT, also known as protein kinase B, is involved in
61 the control of cell survival and metabolism (10), and alterations in the pathway have been observed
62 in tumors and a variety of other diseases (26, 29, 30). More importantly, a prior research has

63 documented the ability of activated AKT pathway to inhibit hepatic gluconeogenesis and
64 adipogenesis in NAFLD mice (36). Here, we inferred that miR-130b-5p was involved in NAFLD
65 through the AKT pathway by targeting IGFBP2. Thus, we developed a NAFLD mouse model
66 induced by HFD, and used this model to test the mechanisms by which miR-130b-5p affects the
67 development of NAFLD through regulation of IGFBP2 and the AKT pathway.

68

69 MATERIALS AND METHODS

70 *Ethics statement*

71 Animal experiments were performed in compliance with the recommendations in the Guide for
72 Treating Experimental Animals of Ministry of Science and Technology of the People's Republic of
73 China (Guo Ke Fa Cai Zi [2006] No. 398) and the Guide for the Care and Use of Laboratory
74 Animals published by the US National Institutes of Health (NIH Publication No. 85-23, revised
75 1996). Extensive efforts were made to minimize the number and discomfort of the included
76 animals.

77

78 *Establishment of NAFLD mouse models*

79 C57BL/6 male mice (aged 5 - 6 weeks, weighing 15 - 18 g) purchased from Guangdong
80 Experimental Animal Center (Guangzhou, China) were fed with standard chow diet (SCD) for 1
81 week. Next, 15 mice were randomly selected to serve as controls, and the remaining mice were fed
82 with HFD (40 kcal% Fat, 20 kcal% Sucrose and 2% Cholesterol) (D09100301, RD Instruments Inc,
83 San Diego, CA, USA) to develop the NAFLD model. All mice were housed with at 22°C and 30-60%
84 relative humidity with a 12-h light/dark cycle. The weight of the mice was recorded weekly.
85 HFD-fed mice were given intraperitoneal injections of 1×10^9 pfu/100 μ L adenoviruses (Shanghai
86 Genechem Co., Ltd., Shanghai, China) expressing knockdown negative control (ad-KD NC),
87 miR-130b-5p knockdown (ad-KD miR-130b-5p), overexpression NC (ad-oe NC), IGFBP2
88 overexpression (ad-oe IGFBP2) or ad-KD miR-130b-5p + IGFBP2 knockdown (ad-KD IGFBP2)

89 twice a week (n = 15 in each group). The infection efficiency was above 80%. At the end of the
90 model induction (on the 8th week of HFD feeding), the mice were anesthetized with 1%
91 pentobarbital sodium and then euthanized by cervical dislocation, after which their liver tissues
92 were collected. Liver tissues from 8 mice were fixed and used for subsequent staining and samples
93 from the other 7 mice were stored at -80°C for subsequent reverse transcription quantitative
94 polymerase chain reaction (RT-qPCR) and Western blot analysis experiments.

95

96 *Oil Red O staining*

97 Oil Red O staining was used to determine cellular lipid droplet formation of liver tissue. The
98 liver tissue was fixed by formalin-calcium solution and cut into 4-μm-thick cryostat slices and
99 stained with 0.5 g oil red O (O8010, Beijing Solarbio Science and Technology Co., Ltd., Beijing,
100 China) for 30 min. Then, the slices were washed using distilled water, counterstained with
101 hematoxylin for 1 min and photographed under an optical microscope (XSP-11CA, Shanghai
102 Optical Instrument Factory, Shanghai, China), with the images obtained.

103

104 *Hematoxylin-eosin (HE) staining*

105 Liver tissue was fixed with 4% paraformaldehyde, embedded in paraffin, and cut into
106 4-μm-thick slices. The slices were then stained with 5% hematoxylin for 10 min, followed by
107 acidification and 5-min staining with eosin. The slices were observed under an optical microscope
108 (XSP-11CA, Shanghai Optical Instrument Factory).

109

110 *RT-qPCR*

111 Total RNA was extracted from liver tissues and cells using TRIzol reagent (15596026, Thermo
112 Fisher Scientific, Waltham, Massachusetts, USA). The primers were designed and synthesized by
113 TaKaRa (Tokyo, Japan). The extracted RNA was reverse transcribed into complementary DNA
114 (cDNA) according to the instructions of a PrimeScriptTM II 1st Strand cDNA Synthesis Kit (for

115 mRNA, TaKaRa) and a miRcute Plus miRNA First-Strand cDNA Synthesis Kit (for miRNA,
116 TIANGEN, Biotechnology Co., Ltd., Beijing, China). The product was stored at -20°C until
117 analysis. RT-qPCR was conducted using the AccessQuick™ RT-PCR System (for mRNA, A1701,
118 Promega, Madison, WI, USA) and a miRcute Plus miRNA qPCR Kit (for miRNA, TIANGEN,
119 Biotechnology Co., Ltd., Beijing, China) according to their respective instructions. The relative
120 expression of miR-130b-5p was standardized relative to U6, while that of the remaining genes by
121 β-actin ([Table 1](#)). The qPCR instrument (Bio-Rad, USA) was used to collect fluorescence signal.
122 The relative expression of target genes was measured using the $2^{-\Delta\Delta Ct}$ method. The experiment was
123 run in triplicate independently.

124

125 *Determination of triglyceride (TG) levels*

126 TG levels were determined using the TG kit (BC0625, Beijing Solarbio Science and
127 Technology Co., Ltd., Beijing, China). The obtained value was normalized to the total protein
128 concentration. The intracellular triglyceride content was expressed in mmol/g protein. Protein
129 concentration was measured using a Pierce™ BCA Protein Assay Kit (23227, Thermo Fisher
130 Scientific Inc., Waltham, Massachusetts, USA).

131

132 *Dual-luciferase reporter assay*

133 Wild type (WT) and mutant (MUT) of IGFBP2 3'-untranslated region (3'UTR) were
134 artificially synthesized and inserted into the luciferase reporter pGL3-control vector (E1741,
135 Promega). Correctly sequenced luciferase reporter plasmids IGFBP2-WT and IGFBP2-MUT were
136 co-transfected into KEK-293T cells with miR-130b-5p mimic and mimic-NC, respectively. After
137 transfection for 48 h, the cells were collected and lysed. Luciferase activity was then measured on a
138 Glomax20/20 luminometer (Promega) using a Dual-Luciferase Reporter Assay System kit
139 (K801-200, Biovision, Milpitas, CA, USA).

140

141 *Western blot analysis*

142 Total protein was extracted from tissues or cells using radioimmunoprecipitation assay (RIPA)
143 (R0010, Beijing Solarbio Science & Technology Co., Ltd., Beijing, China) lysis buffer
144 supplemented with phenylmethylsulphonyl fluoride (PMSF). Supernatant was collected and the
145 protein concentration was determined using a PierceTM BCA Protein Assay Kit (23227, Thermo
146 Fisher Scientific Inc., Waltham, Massachusetts, USA). The isolated 50 µg portions of protein were
147 separated by 10% sodium dodecyl sulfate-polyacrylamide gel electrophoresis, and then transferred
148 to a polyvinylidene fluoride membrane using the wet transfer method. The membrane was blocked
149 with 5% skim milk powder at room temperature for 1 h and then incubated overnight at 4°C with
150 diluted primary rabbit antibodies (Abcam, Cambridge, UK) to IGFBP2 (ab188200, 1:1000), β-actin
151 (ab8227, 1:1000), phosphorylated AKT (S473) (ab81283, 1:5000), AKT (ab179463, 1:1000),
152 phosphorylated mammalian target of rapamycin (mTOR) (S2448) (ab109268, 1:1000) and mTOR
153 (ab2732, 1:2000). On the following day, horseradish peroxidase-labeled secondary antibody against
154 immunoglobulin G (1:1000, Boster Biological Technology Co., Ltd, Wuhan, China) was added to
155 the membrane and incubated at 37°C for 1 h at room temperature. The membrane was developed
156 with enhanced chemiluminescence (ECL) reagent (BB-3501, Amersham, UK). The image was
157 photographed using the Bio-Rad image analysis system (Bio-Rad, Hercules, CA, USA). The band
158 intensities were analyzed using the Quantity One v4.6.2 4.0 software (Media Cybernetics, Maryland,
159 MD, USA). The ratio of the gray value of the bands of interest to those of β-actin was representative
160 of the relative protein expression.

161

162 *Oral glucose tolerance test (OGTT) and insulin tolerance test (ITT)*

163 After 8 weeks of HFD feeding, mice were deprived of food but not water for 12 h. Mice were
164 then subjected with intragastric administration of 2 g/kg glucose (25) and their blood was collected
165 via tail vein at 0, 30, 60, 90, and 120 min later to determine blood glucose levels. Then, mice were
166 intraperitoneally injected with insulin at 0. 1 U/kg and blood was collected via tail vein at 0, 30, 60,

167 90, and 120 min later to determine blood glucose level. A total of 5 μ L of blood was collected and
168 the vital signs of mice were stable during the glucose procedure. Homeostasis model
169 assessment-insulin resistance (HOMA-IR) was finally calculated based on the measured fasting
170 blood glucose (FBG) and fasting insulin (FINS). HOMA-IR = FBG \times FINS/22.5.

171

172 *Enzyme-linked immunosorbent assay (ELISA)*

173 Mouse plasma insulin levels were determined according to the manuals of the insulin ELISA
174 kit (Linco Research Inc., St. Charles, MO, USA) with mouse insulin as the standard.

175

176 *Statistical analysis*

177 All data were processed using SPSS 21.0 statistical software (IBM Corp. Armonk, NY, USA).
178 Measurement data were expressed as mean \pm standard deviation. Data following normal distribution
179 and homogeneity of variance between two groups were compared using unpaired *t*-tests.
180 Comparisons among multiple groups were conducted by one-way analysis of variance (ANOVA)
181 with Tukey's *post hoc* test with corrections for multiple comparisons. Data at different time points
182 were compared by repeated measures ANOVA, followed by Bonferroni *post-hoc* test with
183 corrections for multiple comparisons. A value of $p < 0.05$ indicated significant difference.

184

185 **RESULTS**

186 *IGFBP2 is downregulated in NAFLD mice*

187 We first performed a differential gene expression analysis on NAFLD-associated gene
188 expression datasets (GSE48452, GSE63067 and GSE89632) retrieved from the Gene Expression
189 Omnibus (GEO) database (<https://www.ncbi.nlm.nih.gov/geo>) using R language with $|\log_2$ fold
190 change (FC)| > 2.0 and adj.P.Val < 0.05 set as the threshold for significance. Then, the screened
191 differentially expressed genes (DEGs) were intersected, which showed IGFBP2 to be significantly
192 downregulated in NAFLD (Fig. 1A-D). To further verify the downregulated IGFBP2 in NAFLD in

193 *vivo*, a NAFLD mouse model was generated by HFD feeding. The results showed that body weight
194 gain of HFD-fed mice was markedly accelerated (Fig. 1E), and the liver weight was also
195 significantly elevated at the end of the experiment (Fig. 1F) compared with the SCD-fed mice. HE
196 staining showed significant changes in liver tissues of HFD-fed mice, manifested by hepatocyte
197 volume increase and lipid vacuole dispersion (Fig. 1G). Moreover, the level of TG was notably
198 enhanced in HFD-fed mice (Fig. 1H). These results demonstrated the successful establishment of
199 the NAFLD ARDS mouse model. The results of Western blot analysis and RT-qPCR revealed that
200 IGFBP2 was decreased dramatically in the liver tissues of HFD-fed mice (Fig. 1I, J). Therefore,
201 NAFLD mice exhibited a poor IGFBP2 expression.

202

203 *miR-130b-5p targets IGFBP2*

204 The TargetScan (http://www.targetscan.org/vert_71/), DIANA TOOLS
205 (http://diana.imis.athena-innovation.gr/DianaTools/index.php?r=microT_CDS/index) and miRDB
206 (<http://www.mirdb.org/>) websites predicted binding sites between miR-130b-5p and IGFBP2 (Fig.
207 2A, B). The dual-luciferase reporter assay further verified that miR-130b-5p targeted IGFBP2 (Fig.
208 2C). Meanwhile, RT-qPCR displayed that miR-130b-5p expression was elevated in liver tissues of
209 HFD-fed mice (Fig. 2D). In addition, mRNA expression of IGFBP2 was downregulated upon
210 miR-130b-5p overexpression treatment, while it was increased in the absence of miR-130b-5p (Fig.
211 2E). Western blot analysis also revealed a reduced mRNA expression of IGFBP2 in the presence of
212 miR-130b-5p overexpression, which was abolished by silencing miR-130b-5p (Fig. 2F). The above
213 results demonstrated that miR-130b-5p targeted IGFBP2 and inhibited its expression.

214

215 *Downregulation of miR-130b-5p represses lipid accumulation by upregulating IGFBP2 in NAFLD*
216 *mice*

217 Next, the effect of miR-130b-5p on lipid accumulation was investigated by knocking down
218 miR-130b-5p and altering IGFBP2 in HFD-fed mice. The results of Oil red O staining depicted in

219 Fig. 3A demonstrated significantly increased lipid accumulation in HFD-fed mice compared with
220 the SCD-fed mice, which was reversed by knocking down miR-130b-5p or overexpressing IGFBP2.
221 Moreover, the HFD-fed mice treated with ad-KD miR-130b-5p + ad-KD IGFBP2 had a significant
222 elevation in lipid accumulation compared with the HFD-fed mice treated with ad-KD miR-130b-5p.
223 In addition, the expression of lipid synthesis genes (SREBP-1, LXRa, ChREBP, SCD1, ACC1 and
224 FAS) in liver tissues measured by RT-qPCR exhibited a notably higher trend in the HFD-fed mice
225 than the SCD-fed mice. However, miR-130b-5p knockdown reduced the expression of SREBP-1,
226 LXRa, ChREBP, SCD1, ACC1 and FAS in the liver tissues of HFD-fed mice, which was restored
227 by additional treatment of ad-KD IGFBP2. Similarly, HFD-fed mice treated with ad-oe IGFBP2
228 also presented with a remarkable decline in the expression of SREBP-1, LXRa, ChREBP, SCD1,
229 ACC1 and FAS (Fig. 3B). Therefore, miR-130b-5p increased lipid accumulation through inhibition
230 of IGFBP2 in NAFLD mice.

231

232 *Downregulation of miR-130b-5p alleviates insulin resistance caused by HFD via IGFBP2 in mice*

233 We next attempted to elucidate the role of miR-130b-5p in insulin resistance *in vivo*.
234 miR-130b-5p was knocked down or IGFBP2 was altered in HFD-fed mice by intraperitoneal
235 injections of adenovirus vectors. The body weight and levels of FBG, FINS and HOMA-IR were
236 then measured, which presented that the body weight and levels of FBG, FINS and HOMA-IR were
237 markedly increased in the HFD-fed mice at the 8th week compared with the SCD-fed mice.
238 However, the body weight and levels of FBG, FINS and HOMA-IR were notably reduced in the
239 HFD-fed mice treated with ad-KD miR-130b-5p, which was rescued by IGFBP2 knockdown. In
240 HFD-fed mice treated with ad-oe IGFBP2, a decrease was detected in body weight and levels of
241 FBG, FINS and HOMA-IR (Fig. 4A-D). Additionally, GTT results showed the blood glucose level
242 and area under the curve (AUC) were significantly higher in the HFD-fed mice than those in
243 SCD-fed mice, which was abolished by additional treatment with ad-KD miR-130b-5p or ad-oe
244 IGFBP2. Elevation of blood glucose level and AUC was observed in HFD-fed mice treated with

245 ad-KD miR-130b-5p + ad-KD IGFBP2 in comparison to HFD-fed mice treated with ad-KD
246 miR-130b-5p (Fig. 4E, F). Similar results were also observed following ITT experiments (Fig. 4G,
247 H). The above results serve to illustrate that downregulation of miR-130b-5p reduced the insulin
248 resistance otherwise caused by HFD by upregulating IGFBP2.

249

250 *miR-130b-5p inhibits activation of the AKT pathway via targeting IGFBP2*

251 Finally, to determine that miR-130b-5p could target IGFBP2 to inhibit the AKT pathway, the
252 expression of the AKT pathway-related proteins was detected by Western blot analysis. As
253 displayed in Fig. 5A, B, the expression of IGFBP2 and the extent of AKT/AKT phosphorylation
254 were notably lower in HFD mice than in SCD mice. In HFD-fed mice treated with down-regulated
255 miR-130b-5p or overexpressed IGFBP2, the expression of IGFBP2 and the extent of AKT/AKT
256 phosphorylation was also significantly enhanced. The expression of IGFBP2 and the extent of
257 AKT/AKT phosphorylation were also significantly diminished in HFD-fed mice in response to
258 ad-KD miR-130b-5p + ad-KD IGFBP2 treatment in contrast to ad-KD miR-130b-5p treatment. In
259 conclusion, downregulation of miR-130b-5p increased IGFBP2 expression, thereby mediating
260 activation of the AKT pathway.

261

262 **DISCUSSION**

263 As the number of people with diabetes and obesity increases inexorably in wealthy countries,
264 NAFLD is becoming ever more prevalent, now affecting one in four adults globally (42). Insulin
265 resistance, a hallmark of NAFLD, can promote hepatic lipid accumulation (1). Therefore, finding a
266 possible molecular target of hepatic insulin resistance and lipid accumulation in NAFLD would be
267 clinical significance, and might guide the search for novel treatment for the disease. Existing data
268 have highlighted that abnormal miRNA expression in insulin resistant livers potentially coordinates
269 impaired hepatic metabolic functions (19). Our study evidenced that downregulation of
270 miR-130b-5p prevented lipid accumulation and insulin resistance in NAFLD mice through

271 activation of the AKT pathway by upregulating IGFBP2.

272 First, our data showed that miR-130b-5p was upregulated and IGFBP2 was downregulated in
273 NAFLD mice. A growing number of studies have revealed the upregulation of miR-130b in a
274 variety of diseases. For example, miR-130b is markedly increased in HCC tissues as compared with
275 normal adjacent tissues (27, 34). Human HCC clinical specimens and cell lines also showed
276 overexpression of miR-130b, which is associated with CD133(+) liver tumor initiation, cell growth,
277 and self-renewal (28). Recently derived data indicate that IGFBP2 expression in liver is
278 epigenetically inhibited during hepatic steatosis. Specifically, IGFBP2 expression is reduced in
279 young HFD-induced obesity-susceptible mice (20). Additionally, downregulation of IGFBP2 has
280 been demonstrated in liver tissues of NAFLD mice (3, 18). Those findings supported our present
281 results of high miR-130b-5p expression and poor IGFBP2 expression in NAFLD mouse liver
282 tissues.

283 miRNAs are able to target specific mRNAs and modulate gene expression
284 post-transcriptionally, and are consequently implicated in various biological processes (11, 12). A
285 previous study demonstrated that miR-130b-5p plays an oncogenic role by targeting RASAL1 in
286 gastric cancer cells (9). Additionally, miR-34b-5p has the ability to promote oncogenesis by
287 targeting IGFBP2 in myoblasts (37). These results indirectly supported the results obtained in our
288 study that miR-130b-5p targeted and downregulated IGFBP2. Moreover, our findings also
289 elucidated that miR-130b-5p promoted lipid accumulation and insulin resistance of liver tissues in
290 NAFLD mice by downregulating IGFBP2. Notably, a prior study revealed a correlation of miR-130
291 with adipogenesis (23). miR-130b also possesses an ability to promote obesity-associated adipose
292 tissue inflammation and insulin resistance in diabetic mice by alleviating M2 macrophage
293 polarization *via* repression of PPAR- γ (41). In addition, overexpression of IGFBP2 has been
294 demonstrated to contribute to inhibition of adipogenesis (38) and insulin resistance (24).
295 Furthermore, IGFBP2 can enhance insulin sensitivity in NAFLD (3, 18). The aforementioned
296 evidence suggests the involvement of the miR-34b-5p/IGFBP2 signaling in NAFLD.

297 Another critical finding in our study was that miR-130b-5p inactivated the AKT pathway by
298 targeting IGFBP2. This result was supported by prior studies suggesting that IGFBP2 is capable of
299 activating the AKT pathway (14) and that miR-130b indirectly regulates the AKT pathway in
300 esophageal squamous cell carcinoma cells (39). In addition to those findings, miR-130b is an
301 oncogene overexpressed in osteosarcoma tissues, which has been also found to repress the AKT
302 pathway in those tumor cells (17). Activation of the AKT pathway is conducive to inhibition of
303 gluconeogenesis and lipogenesis in NAFLD (36). Promoting activation of the PI3K/AKT insulin
304 pathway attenuates HFD-induced atherosclerosis and macrophage lipid accumulation (43). What's
305 more, activation of the IGF1-PI3K-AKT/PKB-mTOR pathway has been shown to reduce
306 HFD-induced lipid content and thereby improve skeletal muscle function during resistance training
307 (16). Therefore, miR-130b-5p may be a potential regulator for the AKT pathway by targeting
308 IGFBP2 during NAFLD.

309 All in all, our study suggested that miR-130b-5p promoted lipid accumulation and insulin
310 resistance in NAFLD mice *via* blockade of the AKT pathway by targeting IGFBP2 (Fig. 6). Thus,
311 an investigation of miR-130b-5p along with IGFBP2 and their functions yields a better
312 understanding of their regulatory mechanisms in NAFLD, and may prove to have crucial
313 therapeutic implications in the treatment of NAFLD. Our study provides a rationale for design of a
314 future clinical trial to investigate the efficacy of miR-130b-5p. However, present results also call for
315 investigations in tissue specimens from NAFLD-diagnosed patients for in-depth analysis of the
316 miR-130b-5p/IGFBP2/AKT pathway in human NAFLD.

317

318 **GRANTS**

319 None.

320

321 **DISCLOSURES**

322 No conflicts of interest, financial or otherwise, are declared by the authors.

323

324 **AUTHOR CONTRIBUTIONS**

325 X.N.L. conceived and designed research; X.N.L. and S.H.C. performed experiments; L.J.Z.
326 analyzed data; S.H.C. and L.J.Z. interpreted results of experiments; X.N.L. and L.J.Z. prepared
327 figures; X.N.L. drafted manuscript; S.H.C. and L.J.Z. edited and revised manuscript. All authors
328 approved final version of manuscript.

329

330 REFERENCES

- 331 1. **Abdelmoemen G, Khodeir SA, Zaki AN, Kassab M, Abou-Saif S, Abd-Elsalam S.** Overexpression of
332 Hepassocin in Diabetic Patients with Nonalcoholic Fatty Liver Disease May Facilitate Increased Hepatic Lipid
333 Accumulation. *Endocr Metab Immune Disord Drug Targets* 19: 185-188, 2019.
334 doi:10.2174/187153031866180716100543
- 335 2. **Adams LA, Anstee QM, Tilg H, Targher G.** Non-alcoholic fatty liver disease and its relationship with
336 cardiovascular disease and other extrahepatic diseases. *Gut* 66: 1138-1153, 2017. doi:10.1136/gutjnl-2017-313884
- 337 3. **Ahrens M, Ammerpohl O, von Schonfels W, Kolarova J, Bens S, Itzel T, Teufel A, Herrmann A, Brosch M,**
338 **Hinrichsen H, Erhart W, Egberts J, Sipos B, Schreiber S, Hasler R, Stickel F, Becker T, Krawczak M,**
339 **Rocken C, Siebert R, Schafmayer C, Hampe J.** DNA methylation analysis in nonalcoholic fatty liver disease
340 suggests distinct disease-specific and remodeling signatures after bariatric surgery. *Cell Metab* 18: 296-302, 2013.
341 doi:10.1016/j.cmet.2013.07.004
- 342 4. **Baxter RC.** IGF binding proteins in cancer: mechanistic and clinical insights. *Nat Rev Cancer* 14: 329-341, 2014.
343 doi:10.1038/nrc3720
- 344 5. **Bhatia LS, Curzen NP, Calder PC, Byrne CD.** Non-alcoholic fatty liver disease: a new and important
345 cardiovascular risk factor? *Eur Heart J* 33: 1190-1200, 2012. doi:10.1093/eurheartj/ehr453
- 346 6. **Cermelli S, Ruggieri A, Marrero JA, Ioannou GN, Beretta L.** Circulating microRNAs in patients with chronic
347 hepatitis C and non-alcoholic fatty liver disease. *PLoS One* 6: e23937, 2011. doi:10.1371/journal.pone.0023937
- 348 7. **Chan SH, Wang LH.** Regulation of cancer metastasis by microRNAs. *J Biomed Sci* 22: 9, 2015.
349 doi:10.1186/s12929-015-0113-7.
- 350 8. **Charlton MR, Burns JM, Pedersen RA, Watt KD, Heimbach JK, Dierkhising RA.** Frequency and outcomes
351 of liver transplantation for nonalcoholic steatohepatitis in the United States. *Gastroenterology* 141: 1249-1253,
352 2011. doi:10.1053/j.gastro.2011.06.061
- 353 9. **Chen H, Yang Y, Wang J, Shen D, Zhao J, Yu Q.** miR-130b-5p promotes proliferation, migration and invasion of
354 gastric cancer cells via targeting RASAL1. *Oncol Lett* 15: 6361-6367, 2018. doi:10.3892/ol.2018.8174
- 355 10. **Chen WS, Xu PZ, Gottlob K, Chen ML, Sokol K, Shiyanova T, Roninson I, Weng W, Suzuki R, Tobe K,**
356 **Kadowaki T, Hay N.** Growth retardation and increased apoptosis in mice with homozygous disruption of the Akt1
357 gene. *Genes Dev* 15: 2203-2208, 2001. doi:10.1101/gad.913901
- 358 11. **Chen Y, Wang X.** miRDB: an online database for prediction of functional microRNA targets. *Nucleic Acids Res*
359 10.1093/nar/gkz7572019. doi:10.1093/nar/gkz757
- 360 12. **Corsini LR, Bronte G, Terrasi M, Amodeo V, Fanale D, Fiorentino E, Cicero G, Bazan V, Russo A.** The role
361 of microRNAs in cancer: diagnostic and prognostic biomarkers and targets of therapies. *Expert Opin Ther Targets*
362 16 Suppl 2: S103-109, 2012. doi:10.1517/14728222.2011.650632.
- 363 13. **Di Leva G, Garofalo M, Croce CM.** MicroRNAs in cancer. *Annu Rev Pathol* 9: 287-314, 2014.
364 doi:10.1146/annurev-pathol-012513-104715
- 365 14. **Dunlap SM, Celestino J, Wang H, Jiang R, Holland EC, Fuller GN, Zhang W.** Insulin-like growth factor
366 binding protein 2 promotes glioma development and progression. *Proc Natl Acad Sci U S A* 104: 11736-11741,
367 2007. doi:10.1073/pnas.0703145104
- 368 15. **Feng YY, Xu XQ, Ji CB, Shi CM, Guo XR, Fu JF.** Aberrant hepatic microRNA expression in nonalcoholic fatty
369 liver disease. *Cell Physiol Biochem* 34: 1983-1997, 2014. doi:10.1159/000366394.
- 370 16. **Ferretti R, Moura EG, Dos Santos VC, Caldeira EJ, Conte M, Matsumura CY, Pertille A, Mosqueira M.**
371 High-fat diet suppresses the positive effect of creatine supplementation on skeletal muscle function by reducing
372 protein expression of IGF-PI3K-AKT-mTOR pathway. *PLoS One* 13: e0199728, 2018.
373 doi:10.1371/journal.pone.0199728.
- 374 17. **Han W, Liu J.** LncRNA-p21 inhibited the proliferation of osteosarcoma cells via the miR-130b/PTEN/AKT
375 signaling pathway. *Biomed Pharmacother* 97: 911-918, 2018. doi:10.1016/j.biopha.2017.11.014.
- 376 18. **Hedbacker K, Birsoy K, Wysocki RW, Asilmaz E, Ahima RS, Farooqi IS, Friedman JM.** Antidiabetic effects
377 of IGFBP2, a leptin-regulated gene. *Cell Metab* 11: 11-22, 2010. doi:10.1016/j.cmet.2009.11.007
- 378 19. **Hochreuter MY, Altintas A, Garde C, Emanuelli B, Kahn CR, Zierath JR, Vienberg S, Barres R.**
379 Identification of two microRNA nodes as potential cooperative modulators of liver metabolism. *Hepatol Res* 49:
380 1451-1465, 2019. doi:10.1111/hepr.13419.
- 381 20. **Kammel A, Saussenthaler S, Jahnert M, Jonas W, Stirm L, Hoeflich A, Staiger H, Fritzsche A, Haring HU,**
382 **Joost HG, Schurmann A, Schwenk RW.** Early hypermethylation of hepatic Igfbp2 results in its reduced
383 expression preceding fatty liver in mice. *Hum Mol Genet* 25: 2588-2599, 2016. doi:10.1093/hmg/ddw121.
- 384 21. **Kang HS, Cho HC, Lee JH, Oh GT, Koo SH, Park BH, Lee IK, Choi HS, Song DK, Im SS.** Metformin
385 stimulates IGFBP-2 gene expression through PPARalpha in diabetic states. *Sci Rep* 6: 23665, 2016.
386 doi:10.1038/srep23665.
- 387 22. **Kawano Y, Cohen DE.** Mechanisms of hepatic triglyceride accumulation in non-alcoholic fatty liver disease. *J*
388 *Gastroenterol* 48: 434-441, 2013. doi:10.1007/s00535-013-0758-5

- 389 23. Lee EK, Lee MJ, Abdelmohsen K, Kim W, Kim MM, Srikantan S, Martindale JL, Hutchison ER, Kim HH,
390 Marasa BS, Selimyan R, Egan JM, Smith SR, Fried SK, Gorospe M. miR-130 suppresses adipogenesis by
391 inhibiting peroxisome proliferator-activated receptor gamma expression. *Mol Cell Biol* 31: 626-638, 2011.
392 doi:10.1128/MCB.00894-10
- 393 24. Li Z, Picard F. Modulation of IGFBP2 mRNA expression in white adipose tissue upon aging and obesity. *Horm
394 Metab Res* 42: 787-791, 2010. doi:10.1055/s-0030-1262854
- 395 25. Lim DW, Kim H, Lee SJ, Yu GR, Kim JE, Park WH. Jwa Kum Whan Attenuates Nonalcoholic Fatty Liver
396 Disease by Modulating Glucose Metabolism and the Insulin Signaling Pathway. *Evid Based Complement Alternat
397 Med* 2019: 4589810, 2019. doi:10.1155/2019/4589810
- 398 26. Lin CC, Zhou JP, Liu YP, Liu JJ, Yang XN, Jazag A, Zhang ZP, Guleng B, Ren JL. The silencing of Pokemon
399 attenuates the proliferation of hepatocellular carcinoma cells in vitro and in vivo by inhibiting the PI3K/Akt
400 pathway. *PLoS One* 7: e51916, 2012. doi:10.1371/journal.pone.0051916
- 401 27. Liu AM, Yao TJ, Wang W, Wong KF, Lee NP, Fan ST, Poon RT, Gao C, Luk JM. Circulating miR-15b and
402 miR-130b in serum as potential markers for detecting hepatocellular carcinoma: a retrospective cohort study. *BMJ
403 Open* 2: e000825, 2012. doi:10.1136/bmjopen-2012-000825
- 404 28. Ma S, Tang KH, Chan YP, Lee TK, Kwan PS, Castilho A, Ng I, Man K, Wong N, To KF, Zheng BJ, Lai PB,
405 Lo CM, Chan KW, Guan XY. miR-130b Promotes CD133(+) liver tumor-initiating cell growth and self-renewal
406 via tumor protein 53-induced nuclear protein 1. *Cell Stem Cell* 7: 694-707, 2010. doi:10.1016/j.stem.2010.11.010
- 407 29. Opel D, Naumann I, Schneider M, Bertele D, Debatin KM, Fulda S. Targeting aberrant PI3K/Akt activation by
408 PI103 restores sensitivity to TRAIL-induced apoptosis in neuroblastoma. *Clin Cancer Res* 17: 3233-3247, 2011.
409 doi:10.1158/1078-0432.CCR-10-2530
- 410 30. Ramaswamy B, Lu Y, Teng KY, Nuovo G, Li X, Shapiro CL, Majumder S. Hedgehog signaling is a novel
411 therapeutic target in tamoxifen-resistant breast cancer aberrantly activated by PI3K/AKT pathway. *Cancer Res* 72:
412 5048-5059, 2012. doi:10.1158/0008-5472.CAN-12-1248
- 413 31. Safari Z, Gerard P. The links between the gut microbiome and non-alcoholic fatty liver disease (NAFLD). *Cell
414 Mol Life Sci* 76: 1541-1558, 2019. doi:10.1007/s00018-019-03011-w
- 415 32. Santhekadur PK, Kumar DP, Sanyal AJ. Preclinical models of non-alcoholic fatty liver disease. *J Hepatol* 68:
416 230-237, 2018. doi:10.1016/j.jhep.2017.10.031
- 417 33. Starley BQ, Calcagno CJ, Harrison SA. Nonalcoholic fatty liver disease and hepatocellular carcinoma: a
418 weighty connection. *Hepatology* 51: 1820-1832, 2010. doi:10.1002/hep.23594
- 419 34. Tu K, Zheng X, Dou C, Li C, Yang W, Yao Y, Liu Q. MicroRNA-130b promotes cell aggressiveness by
420 inhibiting peroxisome proliferator-activated receptor gamma in human hepatocellular carcinoma. *Int J Mol Sci* 15:
421 20486-20499, 2014. doi:10.3390/ijms15120486
- 422 35. Wagschal A, Najafi-Shoushtari SH, Wang L, Goedeke L, Sinha S, deLemos AS, Black JC, Ramirez CM, Li Y,
423 Tewhey R, Hatoum I, Shah N, Lu Y, Kristo F, Psychogios N, Vrbanac V, Lu YC, Hla T, de Cabo R, Tsang JS,
424 Schadt E, Sabeti PC, Kathiresan S, Cohen DE, Whetstone J, Chung RT, Fernandez-Hernando C, Kaplan
425 LM, Bernards A, Gerszten RE, Naar AM. Genome-wide identification of microRNAs regulating cholesterol and
426 triglyceride homeostasis. *Nat Med* 21: 1290-1297, 2015. doi:10.1038/nm.3980
- 427 36. Wang C, Chi Y, Li J, Miao Y, Li S, Su W, Jia S, Chen Z, Du S, Zhang X, Zhou Y, Wu W, Zhu M, Wang Z,
428 Yang H, Xu G, Wang S, Yang J, Guan Y. FAM3A activates PI3K p110alpha/Akt signaling to ameliorate hepatic
429 gluconeogenesis and lipogenesis. *Hepatology* 59: 1779-1790, 2014. doi:10.1002/hep.26945
- 430 37. Wang Z, Zhang X, Li Z, Abdalla BA, Chen Y, Nie Q. MiR-34b-5p Mediates the Proliferation and Differentiation
431 of Myoblasts by Targeting IGFBP2. *Cells* 8: 2019. doi:10.3390/cells8040360
- 432 38. Xi G, Solum MA, Wai C, Maile LA, Rosen CJ, Clemons DR. The heparin-binding domains of IGFBP-2
433 mediate its inhibitory effect on preadipocyte differentiation and fat development in male mice. *Endocrinology* 154:
434 4146-4157, 2013. doi:10.1210/en.2013-1236
- 435 39. Yu T, Cao R, Li S, Fu M, Ren L, Chen W, Zhu H, Zhan Q, Shi R. MiR-130b plays an oncogenic role by
436 repressing PTEN expression in esophageal squamous cell carcinoma cells. *BMC Cancer* 15: 29, 2015.
437 doi:10.1186/s12885-015-1031-5
- 438 40. Zarrinpar A, Gupta S, Maurya MR, Subramaniam S, Loomba R. Serum microRNAs explain discordance of
439 non-alcoholic fatty liver disease in monozygotic and dizygotic twins: a prospective study. *Gut* 65: 1546-1554, 2016.
440 doi:10.1136/gutjnl-2015-309456
- 441 41. Zhang M, Zhou Z, Wang J, Li S. MiR-130b promotes obesity associated adipose tissue inflammation and insulin
442 resistance in diabetes mice through alleviating M2 macrophage polarization via repression of PPAR-gamma.
443 *Immunol Lett* 180: 1-8, 2016. doi:10.1016/j.imlet.2016.10.004.
- 444 42. Zhou JH, Cai JJ, She ZG, Li HL. Noninvasive evaluation of nonalcoholic fatty liver disease: Current evidence
445 and practice. *World J Gastroenterol* 25: 1307-1326, 2019. doi:10.3748/wjg.v25.i11.1307
- 446 43. Zhou M, Ren P, Li S, Kang Q, Zhang Y, Liu W, Shang J, Gong Y, Liu H. Danhong Injection Attenuates
447 High-Fat-Induced Atherosclerosis and Macrophage Lipid Accumulation by Regulating the PI3K/AKT Insulin
448 Pathway. *J Cardiovasc Pharmacol* 74: 152-161, 2019. doi:10.1097/FJC.0000000000000691.
- 449

450 **LEGENDS**

451 **Fig. 1.** IGFBP2 shows poor expression in NAFLD. A, Intersected NAFLD-related DEGs analyzed
452 from the GSE48452, GSE63067 and GSE89632 datasets. The number in the color circle represents
453 the number of NAFLD-related genes in each dataset. B-D, The expression of IGFBP2 analyzed
454 from the GSE48452, GSE63067 and GSE89632 datasets. The Y-axis represents the relative
455 expression of IGFBP2 normalized to its housekeeping gene. E, Weekly mouse body weight during
456 the establishment of mouse models of NAFLD. F, Liver weight of mice at the 8th week of HFD
457 feeding. G, HE staining of mouse liver tissue and oil red O staining of lipid accumulation in liver
458 tissue ($\times 400$). H, TG levels in mice. I, mRNA expression of IGFBP2 in liver tissues detected by
459 RT-qPCR, normalized to β -actin. J, The protein expression of IGFBP2 in mouse liver tissue
460 measured by Western blot analysis, normalized to β -actin. * $p < 0.05$ vs. SCD-fed mice.
461 Measurement data (mean \pm standard deviation) between two groups were analyzed by unpaired
462 *t*-test, and those at different time points were compared by repeated measures ANOVA, followed by
463 Bonferroni *post hoc* test. n = 15 for HFD-fed and SCD-fed mice.

464 **Fig. 2.** IGFBP2 is a target gene of miR-130b-5p. A, The intersected miRNAs regulating IGFBP2
465 predicted by the TargetScan, miRDB and DIANA TOOLS websites. The number in the color circle
466 represents the number of miRNAs regulating IGFBP2 in the three websites. B, Binding sites
467 between miR-130b-5p and IGFBP2 predicted by the TargetScan, miRDB and DIANA TOOLS. C,
468 The binding of miR-130b-5p to IGFBP2 verified using dual-luciferase reporter assay. * $p < 0.05$ vs.
469 NC mimic-treated mice; # $p < 0.05$ vs. inhibitor NC-treated mice. D, Expression of miR-130b-5p in
470 mouse liver tissues determined by RT-qPCR, normalized to U6. E, miR-130b-5p expression and
471 IGFBP2 mRNA expression in liver tissues of HFD-fed mice treated with miR-130b-5p agomir or
472 ad-KD miR-130b-5p determined by RT-qPCR, normalized to U6 and β -actin, respectively. F, The
473 protein expression of IGFBP2 in liver tissues of HFD-fed mice treated with miR-130b-5p agomir or
474 ad-KD miR-130b-5p measured by Western blot analysis, normalized to β -actin. * $p < 0.05$ vs.
475 HFD-fed mice treated with agomir NC; # $p < 0.05$ vs. HFD-fed mice treated with ad-KD-NC.

476 Measurement data (mean \pm standard deviation) were analyzed by unpaired *t*-test. n = 15 for
477 HFD-fed and SCD-fed mice.

478 **Fig. 3.** miR-130b-5p downregulation reduces lipid accumulation *via* IGFBP2 upregulation in
479 NAFLD mice. SCD-fed mice were utilized as control, and HFD-fed mice were injected with
480 adenoviruses carrying ad-KD NC, ad-KD miR-130b-5p, ad-oe IGFBP2, ad-oe NC or ad-KD
481 miR-130b-5p + ad-KD IGFBP2. A, Lipid accumulation in mouse liver tissues detected by Oil Red
482 O staining (\times 200). B, Expression of lipid synthesis-related genes (SREBP-1, LXRa, ChREBP,
483 SCD1, ACC1 and FAS) in mouse liver tissues measured by RT-qPCR, normalized to β -actin. * *p* <
484 0.05 vs. SCD-fed mice, # *p* < 0.05 vs. HFD-fed mice treated with ad-KD NC, & *p* < 0.05 vs.
485 HFD-fed mice treated with ad-oe NC, @ *p* < 0.05 vs. HFD-fed mice treated with ad-KD
486 miR-130b-5p. Measurement data (mean \pm standard deviation) were compared by one-way ANOVA
487 with Tukey's *post hoc* test. n = 15 for mice following each treatment.

488 **Fig. 4.** Knockdown of miR-130b-5p targets IGFBP2 to suppress insulin resistance in NAFLD mice.
489 SCD-fed mice were utilized as control, and HFD-fed mice were injected with adenoviruses carrying
490 ad-KD NC, ad-KD miR-130b-5p, ad-oe IGFBP2, ad-oe NC or ad-KD miR-130b-5p + ad-KD
491 IGFBP2. A, Body weight of mice at different time points. B, FBG levels of mice after starving for
492 12 h. C, FINS levels of mice after starving for 12 h. D, HOMA-IR levels of mice. E, Blood glucose
493 levels of mice detected by GGT. F, AUC corresponding to panel E. G, Blood glucose levels of mice
494 determined by ITT. H, AUC corresponding to panel G. * *p* < 0.05 vs. SCD-fed mice, # *p* < 0.05 vs.
495 HFD-fed mice treated with ad-KD NC, & *p* < 0.05 vs. HFD-fed mice treated with ad-oe NC, @ *p* <
496 0.05 vs. HFD-fed mice treated with ad-KD miR-130b-5p. Measurement data (mean \pm standard
497 deviation) among multiple groups were compared by one-way ANOVA with Tukey's *post hoc* test,
498 and those at different time points were compared by repeated measures ANOVA, followed by
499 Bonferroni *post hoc* test. n = 15 for mice following each treatment.

500 **Fig. 5.** miR-130b-5p disrupts activation of the AKT pathway *via* inhibition of IGFBP2. SCD-fed
501 mice were utilized as control, and HFD-fed mice were injected with adenoviruses of ad-KD NC,

502 ad-KD miR-130b-5p, ad-oe IGFBP2, ad-oe NC or ad-KD miR-130b-5p + ad-KD IGFBP2. A, The
503 protein expression of IGFBP2, AKT and p-AKT in mice detected by Western blot analysis,
504 normalized to β -actin. B, Quantification results of panel A. * $p < 0.05$ vs. SCD-fed mice, # $p < 0.05$
505 vs. HFD-fed mice treated with ad-KD NC, & $p < 0.05$ vs. HFD-fed mice treated with ad-oe NC, @
506 $p < 0.05$ vs. HFD-fed mice treated with ad-KD miR-130b-5p. Measurement data (mean \pm standard
507 deviation) among multiple groups were compared by one-way ANOVA with Tukey's *post hoc* test.
508 n = 15 for mice following each treatment.

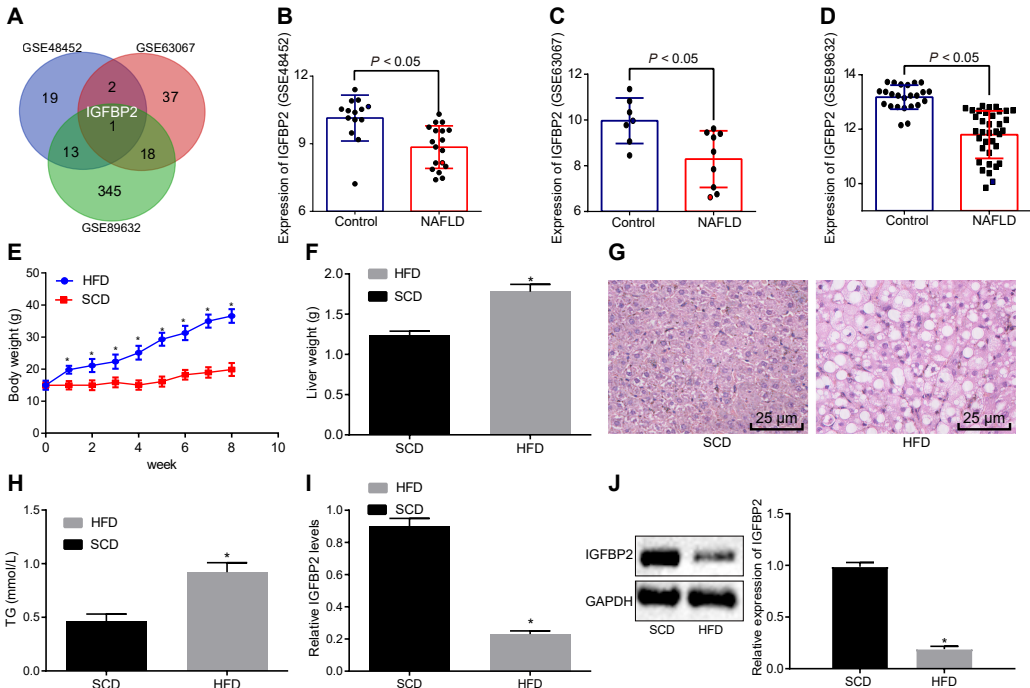
509 **Fig. 6.** A mechanism map depicting the role of miR-130b-5p in NAFLD *via* IGFBP2. miR-130b-5p
510 could target IGFBP2, and IGFBP2 activated the AKT pathway and phosphorylated AKT. Activation
511 of the AKT pathway inhibited the expression of the lipid synthesis genes including SREBP-1,
512 LXRa, ChREBP, SCD1, ACC1 and FAS, thereby inhibiting lipid accumulation and insulin
513 resistance in NAFLD.

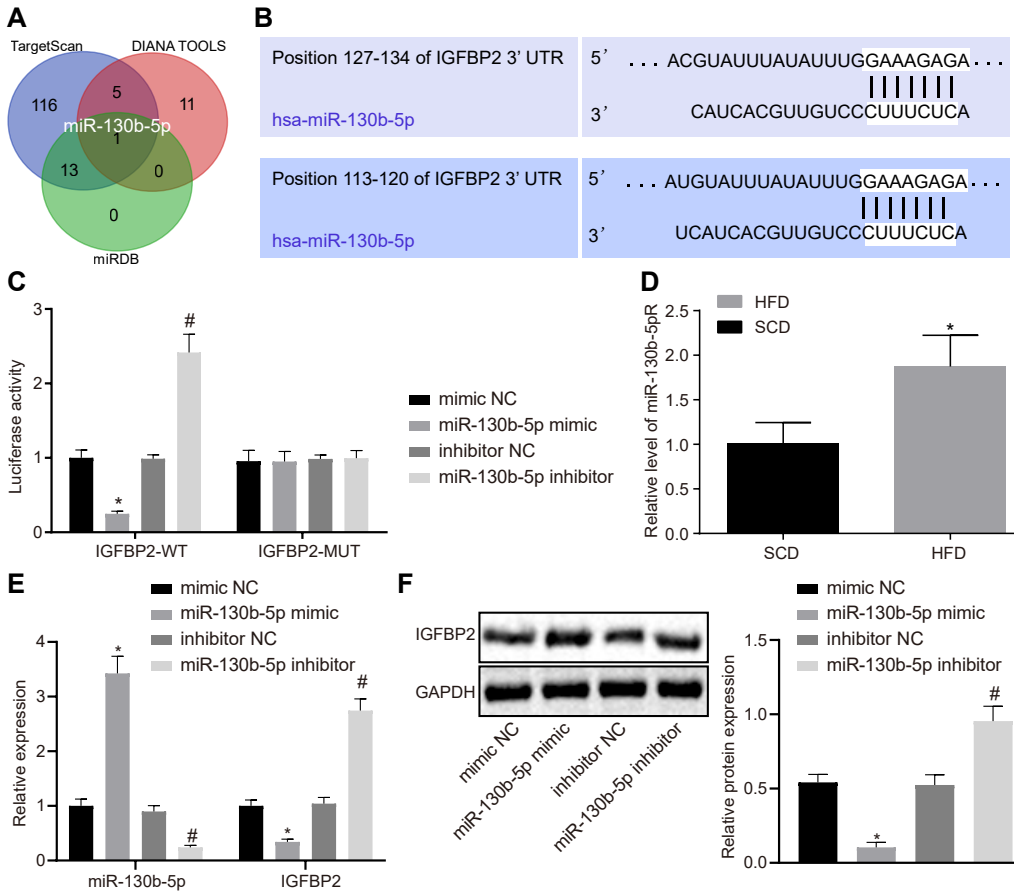
514

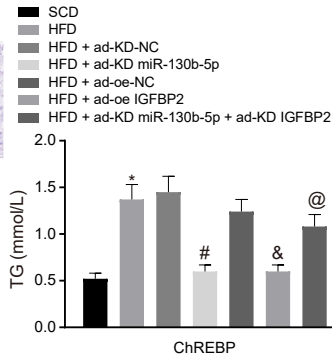
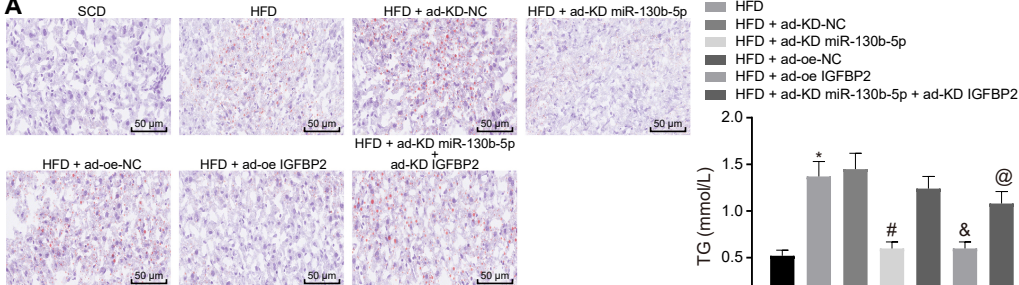
Table 1 Primer sequences for RT-qPCR

Gene	Primer sequence
IGFBP2	F: 5'-TGGTTGCAGACAATGGCGATTCAAGAACATGCCATTGTCTGCAACCTTTTC-3' R: 5' TCGAGAAAAAAGGTTGCAGAACAAATGGGGATTCTCTTGAATGCCATTGTCTGCAACCA-3'
miR-130b-5p	F: 5'-GCGCCTCATCACGTTGCCCTTCTCA-3' R: 5'-GTGCAGGGTCCGAGGT-3'
β-actin	F: 5'- TGGGAATGGGTAGAACAGGA-3' R: 5'- ATTGAGAAAGGGGGTGGC-3'
U6	F: 5'-GCTTCGGCAGCACATATAACTAAAAT-3' R: 5'-CGCTTCACGAATTGCGTGTAT-3'
SREBP-1	F: 5'-GGAGCCATGGATTGCACATT-3' R: 5'-GCTTCCACAGAGGGAGGCCAG-3'
LXRa	F: 5'-TTGCTTCAGCTCACAGAGA-3' R: 5'-TGGTTGTAGAGGGCAAGGAC-3'
ChREBP	F: 5'-CCCTCAGACACCCACTCTT-3' R: 5'-CAGAGCTCAGAAAGGGTTG-3'
SCD1	F: 5'-TGGGGCTGCTAATCTCTGGGTGTA-3' R: 5'-GGCTTATCTCTGGGTGGGTTG-3'
ACC1	F: 5'-TGAATCTVACGCGCTACTAT-3' R: 5'-ATGACCVTGTTGCCTCAAAC-3'
FAS	F: 5'-CGCCTATGGTTGACC-3' R: 5'-CCTCTGTTACAGACCTC-3'

Note: RT-qPCR, reverse transcription quantitative polymerase chain reaction; IGFBP2, insulin-like growth factor binding protein 2; miR-130b-5p, microRNA-130b-5p; SREBP-1, sterol regulatory element-binding protein 1; LXRa, liver X receptor alpha; ChREBP, carbohydrate-responsive element-binding protein; SCD1, stearoyl CoA desaturase 1; ACC1, acetyl CoA carboxylase 1; FAS, fatty acid synthase; F, forward; R, reverse.



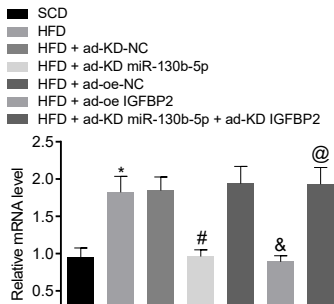


A**B**

SREBP-1



LXra



SCD1



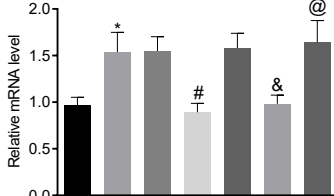
ACC1



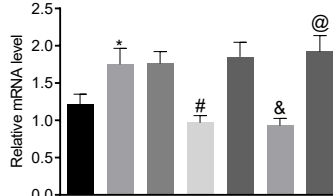
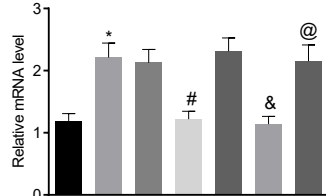
FAS

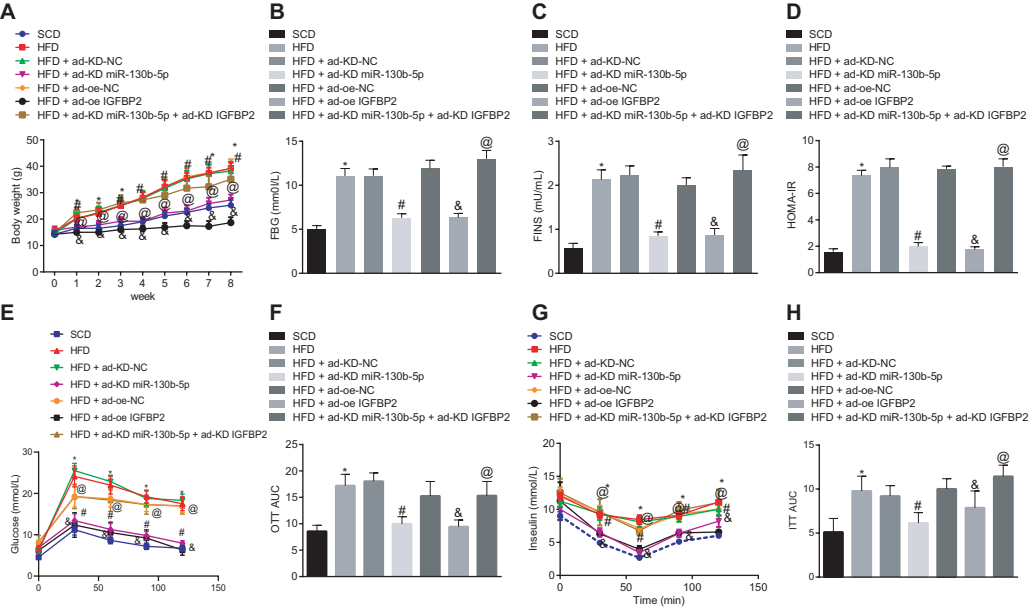


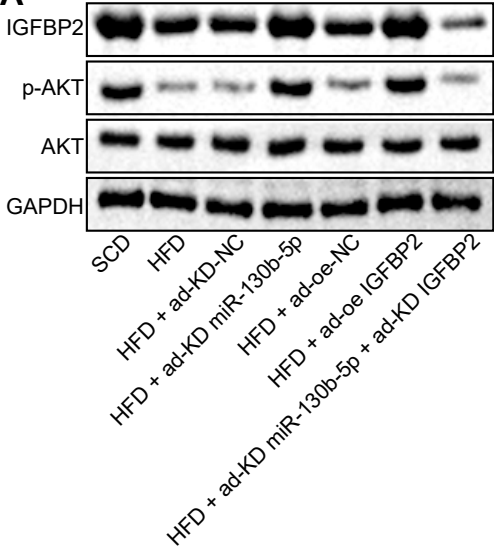
HIF1α



IGFBP2





A**B**